IEEE Access
Multidisciplinary | Rapid Review | Open Access Journal

Received 1 January 2024, accepted 20 January 2024, date of publication 23 January 2024, date of current version 31 January 2024.

Digital Object Identifier 10.1109/ACCESS.2024.3357617

RESEARCH ARTICLE

A Calculation Method for the Maximum Transmission Power in ICPT Systems Under Non-Sinusoidal Excitation

YUE XU, KAI XIE, AND YAN LIU
School of Aerospace Science and Technology, Xidian University, Xi'an 710071, China
Corresponding author: Yue Xu (yxu_95@stu.xidian.edu.cn)

ABSTRACT Calculating the maximum transmission power of loosely coupled coils represents a crucial step in the design of inductively coupled power transfer (ICPT) systems. However, the majority of calculations for the maximum power transfer point (MPTP) are exclusively relevant to scenarios featuring pure sinusoidal excitation. This paper introduces a more universally applicable solution for determining the MPTP in loosely coupled systems subjected to arbitrary excitations. The approach takes into account the contributions of both the fundamental waveform and all harmonics to the transmission capacity, offering a precise method for investigating the maximum power capacity of ICPT systems under non-sinusoidal excitation. Through simulations and experiments, it is demonstrated that the proposed method yields improved agreement with various waveform excitations, including square/triangular waves, as well as actual chopping waves characterized by large-scale ringing and overshoot. The versatility of the method extends to various inductively coupled systems with generic excitations, encompassing non-resonant-type, direct chopper, or multi-level inverter-driven ICPT systems. Furthermore, the method ensures greater accuracy in instances of excitation distortion induced by nonlinear effects.

INDEX TERMS ICPT, maximum power transfer, non-sinusoidal, wireless power transmission.

I. INTRODUCTION

Inductively coupled power transfer (ICPT) stands as a pivotal means to achieve wireless, non-contact electrical energy transmission, particularly suitable for short-distance power transfer that requires frictionless, explosion-proof, moisture-proof, and waterproof capabilities. In ICPT systems, coupled inductors are employed to convey energy from a transmitter coil to a receiver coil, with power transfer executed through an alternating magnetic field as the medium [1]. This transmission method alleviates challenges associated with disorderly power lines, addresses the security limitations of conventional power supply methods, and offers increased flexibility. ICPT finds widespread application in various domains, including power supplies for underwater machinery [2], [3], consumer electronics [4], medical implants [5], [6], and electric vehicles [7], [8].

The associate editor coordinating the review of this manuscript and approving it for publication was Kai Song.

The design of the magnetic coupler in the ICPT system holds paramount importance as it profoundly affects the power transfer capability of the entire system, showcasing the attributes of weakly correlated coupling [9]. This loosely coupled nature implies that the load can only attain maximum power—specifically, the maximum power of the loosely coupled system—when the load impedance aligns with the leakage reactance [10].

The maximum transmission power serves as a defining attribute for the power transmission capability of ICPT systems and constitutes a pivotal performance indicator for the overall system. Its significance is heightened when estimating both the power transmission capacity of ICPT systems [11] and the switching threshold for multi-mode coupled power transmission [12]. Resolving these issues and optimizing subsequent power transmissions necessitates the determination of a physical interpretation of the maximum transmitted power and the prediction of the maximum power transfer point (MPTP). Additionally, delving into these aspects not

only offers theoretical support for normalization technology (the ratio of actual transmission power to maximum transmission power) but also for understanding the characteristics of the maximum power transmission. This research proves instrumental in enhancing system performance and stability.

Sinusoidal voltages are frequently employed for excitation in these studies, primarily due to their prevalent use in magnetically coupled resonant wireless power transfer systems [13]. Upon compensation, when the system achieves resonance, the voltage waveform applied to the primary coil closely approximates a sine wave. In instances of such sinusoidal excitation, the system's output voltage and power can be calculated using sinusoidal steady-state theory. A distinct method for calculating the transmission capacity of the system has been proposed [14].

However, in numerous practical application scenarios, non-sinusoidal waves emerge as the preferred excitation waveforms for ICPT systems. For example, in specific industrial control fields, the shape and spectral characteristics of non-sine waves more readily conform to actual working conditions, thereby improving the system's control accuracy and response speed [15], [16], [17]. In medical equipment, semiconductor production equipment, and various other domains [18], [19], [20], the use of non-sinusoidal waves for excitation allows for better adaptation to load changes. Fine-tuned control is achievable by adjusting parameters such as wave frequency, amplitude, and phase, ensuring the system's accuracy and stability. In applications demanding high-efficiency conversions, such as power electronics and lighting [21], [22], non-sinusoidal waves prove advantageous in optimizing power factors and minimizing losses, thereby improving energy efficiency. Additionally, in simple or low-cost devices [23], [24], [25], the input voltage waveforms of the magnetic elements and switching elements often take the form of non-sinusoidal waves, such as square waves and pulse width modulation waveforms. Pulse square waves, for instance, carry higher energy than sine waves [26]. In addition, the use of a non-sinusoidal wave as the power supply voltage results in heightened power efficiency [27].

In the aforementioned studies and applications, it is imperative to delve into aspects such as the calculation and tracking of maximum power. A notable example is the investigation into the power and efficiency characteristics of electric vehicle wireless charging systems relying on non-sinusoidal inputs [28]. In scenarios characterized by highly non-sinusoidal conditions, the precise determination of the power delivered to the load becomes essential.

However, in the aforementioned circumstances, utilizing the calculation method for the sinusoidal steady-state MPTP from traditional theory can introduce unpredictable errors. The potential adverse effects of these errors include overloading the receiver load, resulting in device damage or compromising system stability [29], [30]. This can lead to reduced transmission efficiency, energy wastage, or compromised overall system performance [31], [32]. Furthermore, these effects may impact the design of components such as couplers, causing errors in tracking and compensation circuits [33], [34], [35], [36], [37].

Therefore, in inductively coupled wireless power transfer, precision in calculating the maximum power that the load can acquire at the receiver is imperative. This information is essential for effective system design and control. In scenarios involving non-sinusoidal excitation, there exists a compelling need to devise methods for accurately calculating the maximum power attainable by the receiver's load in ICPT systems.

This paper introduces a methodology for determining the MPTP in ICPT systems operating under non-sinusoidal excitation. The approach considers the contribution of each high-frequency harmonic to the maximum power achievable by the load, facilitating swift and accurate determination of the MPTP for the ICPT system.

II. PROBLEM FORMULATION

A. MPTP IN SINUSOIDAL ICPT SYSTEM

The principal distinction between wireless power transfer systems and traditional power supply systems lies in the former's loosely coupled nature. In an ICPT system, power transfer is based on a loosely coupled structure using a pair of coils. As a result, not all of the primary flux and secondary flux are fully coupled, inevitably resulting in leakage inductance. In general, the load cannot receive the maximum power provided by the system, and the system itself consumes substantial amounts of energy to maintain the operation of the energy transfer magnetic field. The leakage inductance in the system's primary and secondary load circuits is equivalent to the series component of the voltage and inductance. Although this inductance does not consume power, it restricts the currents in the primary excitation circuit and the secondary load circuit, thereby limiting the maximum power that the load can obtain. Fig. 1 shows an equivalent circuit diagram for a typical ICPT system.

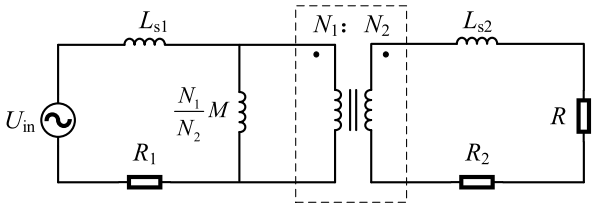

FIGURE 1. Schematic of loosely coupled structure.

In Fig. 1, U_{in} and R represent the system's supply voltage and load resistance, respectively. N_1 and N_2 denote the number of turns in the coils of the primary and secondary loops, respectively. R_1 and R_2 are the impedances of the primary and secondary loops, while L_{s1} and L_{s2} are the leakage inductances in the primary and secondary loops, respectively. M denotes the mutual inductance between the two loops.

The model is subject to the following constraint relationships:

$$\begin{cases} \dfrac{N_1}{N_2}M = KL_1 \\ L_{s1} = (1-K)\,L_1 \\ L_{s2} = (1-K)\,L_2 \end{cases} \tag{1}$$

where L_1 and L_2 are the inductances of the primary and secondary loops, respectively, and K represents the coupling coefficient between these two loops. The primary excitation and loop impedance can be reflected to the corresponding secondary values, leading to the derivation of the equivalent circuit, as shown in Fig. 2.

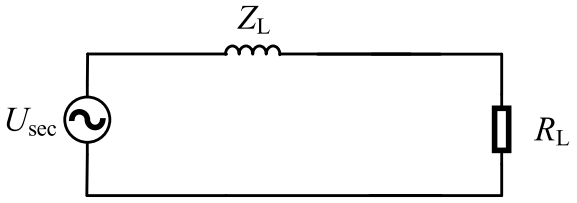

FIGURE 2. Equivalent circuit schematic (reflected to secondary side).

As shown in Fig. 2, U_{sec} is the primary equivalent voltage, Z_L is the combined equivalent impedance reflected from the primary side and the secondary impedance, and N denotes the turn ratio of the secondary and primary loops. According to Kirchhoff's voltage law (KVL), the impedance and voltage reflected from the primary circuit to the secondary circuit can be expressed as:

$$\begin{cases} Z_L = N^2 j\omega K L_{s1} + j\omega L_{s2} + N^2 K R_1 + R_2 \\ U_{sec} = NK\,U_{\text{in}} \end{cases} \tag{2}$$

For ease of calculation, all resistive components, including coil impedance, are integrated into R_L. Therefore, the inductive impedance Z_{Lm} can be simplified as follows:

$$Z_{Lm} = N^2 j\omega K L_{s1} + j\omega L_{s2} \tag{3}$$

The loosely coupled transformer exhibits a leakage inductance, causing K to consistently be less than 1. The impedance of this leakage inductance is distributed with the load, resulting in a voltage loss in the output. Maximum power occurs when the load and leakage inductances are equal. Further reduction of the load resistance does not result in increased power output. This fundamental characteristic differs significantly from a tightly coupled system.

Under sinusoidal excitation, the MPTP load resistance $Z_{\text{Lm(sin)}}$ and the maximum power $P_{\text{om(sin)}}$ can be described as follows:

$$Z_{\text{Lm(sin)}} = N^2\left(1-K^2\right)\omega L_1 \tag{4a}$$

$$P_{\text{om(sin)}} = \frac{N^2 K^2 U_{\text{in}}^2}{2\left|Z_{Lm(\text{sin})}\right|} \tag{4b}$$

Due to the presence of an air gap in the loosely coupled transformer, the coupling coefficient K is less than 1, resulting in the existence of leakage inductance. The reactance of this leakage inductance interacts with the load impedance, thereby limiting the maximum output power. Maximum power is achieved when the load impedance matches the reactance of the leakage inductance, and further reduction of the load resistance does not yield increased power.

It is important to note that Eq. (4) is applicable only under sinusoidal conditions. In the non-sinusoidal case, using Eq. (4) leads to the calculation of higher harmonics as if they were the same as the fundamental frequency. This discrepancy causes the calculated value of $Z_{\text{Lm(sin)}}$ to deviate from the actual value, rendering the value of $P_{\text{om(sin)}}$ inaccurate. To ensure accurate calculations under non-sinusoidal conditions, it is imperative to consider the attenuation of each harmonic component.

B. MPTP IN NON-SINUSOIDAL SYSTEM

In many practical applications, generating non-sinusoidal excitation is more convenient, and square pulse waves carry more energy than sinusoidal waves. Therefore, in the aforementioned scenario, persisting with the sinusoidal steady-state method from traditional theory would lead to a deviation between the calculated MPTP and the actual value. To ascertain the general characteristics of the MPTP in the ICPT system and predict the MPTP accurately, the impact of the leakage inductance on each frequency component of the fundamental and higher harmonic transmission components in the loosely coupled structure will be discussed in the following.

A continuous non-sinusoidal waveform can be decomposed into multiple sinusoidal signals in a harmonic relationship through an expansion based on Fourier transformation.

A non-sinusoidal excitation voltage $u(t)$ with a period T can be expressed as an infinite series based on the Fourier transform rules:

$$u\,(t) = a_0 + \sum_{\text{n}=1}^{\infty}\left[a_{\text{n}}\cos\left(\frac{2\pi nt}{T}\right) + b_{\text{n}}\sin\left(\frac{2\pi nt}{T}\right)\right] \tag{5}$$

where the Fourier coefficients are:

$$\begin{cases} a_0 = \dfrac{1}{T}\displaystyle\int_{t_0}^{t_0+T} u\,(t)\,dt \\ a_{\text{n}} = \dfrac{2}{T}\displaystyle\int_{t_0}^{t_0+T} u(t)\cos\left(\dfrac{2\pi nt}{T}\right)dt,\ n=1,2,3\cdots \\ b_{\text{n}} = \dfrac{2}{T}\displaystyle\int_{t_0}^{t_0+T} u(t)\sin\left(\dfrac{2\pi nt}{T}\right)dt,\ n=1,2,3\cdots \end{cases} \tag{6}$$

If the sine and cosine components of the same frequency are combined, the voltage excitation can then be expanded into the form of a sum of the series of the fundamental and

multiple harmonics. The Fourier series can be expressed as:

$$U(t) = A_0 + \sum_{n=1}^{\infty} A_n \sin(n\omega t + \varphi_n) \tag{7}$$

where

$$\begin{cases} A_n = \sqrt{a_n^2 + b_n^2} \\ \varphi = \arctan(b_n / a_n) \end{cases} \tag{8}$$

Here, ω is the fundamental frequency, and $n\omega$ is the n^{th} harmonic frequency. In Eq. (7), A_0 represents the DC component, which cannot pass through the transformer. In the MPTP correction, however, A_0 can be omitted. For each harmonic component, the voltage obtained across R_L is:

$$U_n = U_{sec} \frac{R_L}{R_L + jn\omega L_h} = U_{sec} \frac{R_L}{R_L + jn\omega N^2(1-K^2)L_1} \tag{9}$$

For the nth harmonic component, the power obtained on R_L is:

$$P_n = \frac{|U_n|^2}{2R_L} = \frac{U_{sec}^2 R_L}{2\left[R_L^2 + n^2\omega^2 N^4 (1-K^2)^2 L_1^2\right]} \tag{10}$$

Because each frequency component is orthogonal, the total power obtained on the load is:

$$P_L = \sum_{n=1}^{\infty} P_n = \sum_{n=1}^{\infty} A_n^2 \frac{N^2 K^2 R_L}{2\left[R_L^2 + n^2\omega^2 N^4 (1-K^2)^2 L_1^2\right]} \tag{11}$$

Eq. (11) indicates that the MPTP is dependent on the harmonic components. By employing the steepest gradient descent method to conduct a one-dimensional search on the total power P_L in the equation, we can determine the maximum power value and the load impedance value at the MPTP.

In practical scenarios, for an approximate numerical solution, considering the first m terms, the sum of the powers of the first m terms is given by:

$$P_{Lm} = \sum_{n=1}^{m} \frac{N^2 K^2 A_n^2 R_L}{2\left[R_L^2 + n^2\omega^2 N^4 \left(1-K^2\right)^2 L_1^2\right]} \tag{12}$$

This method of approximate solution introduces computational errors, and the residual E_m can be expressed as:

$$E_m = (P_L - P_{Lm})/P_L \times 100\% \tag{13}$$

The relative power truncation error of the non-sinusoidal signal after truncating m terms is given by:

$$e_m = \left[\sum_{n=m+1}^{\infty} \left(a_n^2 + b_n^2\right) \Big/ \sum_{n=1}^{\infty} \left(a_n^2 + b_n^2\right)\right] \times 100\% \tag{14}$$

Since the input power of the signal is known, Equation (14) can be calculated using the following formula.

$$e_m = 1 - \frac{1}{2} \sum_{n=1}^{m} \left(a_n^2 + b_n^2\right) \Big/ \frac{1}{T} \int_0^T |u(t)|^2 \, dt \times 100\% \tag{15}$$

Due to the fact that $E_m < e_m$, the calculation accuracy can be determined based on Eq. (15), and m can be determined according to the desired accuracy in Eq. (15). Subsequently, the calculation of the maximum power is performed.

C. MPTP IN COMMON DRIVE WAVEFORMS

First, we analyze commonly used waveforms such as square waves and triangular waves. We study the relationship between the MPTP and the harmonic components, along with the influence of harmonic components on the magnitude of deviation.

For square waves, Eq. (7) can be expanded to give:

$$U(t) = \frac{4U_{in}}{\pi} \left(\sin\omega t + \frac{1}{3}\sin 3\omega t + \frac{1}{5}\sin 5\omega t + \ldots\right) \tag{16}$$

Eq. (11) can be rewritten to give:

$$\begin{aligned} P_{L(sq)} &= \sum_{n=0}^{\infty} \left[\frac{4U_{in}}{(2n+1)\pi}\right]^2 \\ &\quad \times \frac{N^2 K^2 R_L}{2\left[R_L^2 + (2n+1)^2\omega^2 N^4 (1-K^2)^2 L_1^2\right]} \\ &= \frac{8N^2K^2U_{in}^2}{\pi^2} \sum_{n=0}^{\infty} \left(\frac{1}{2n+1}\right)^2 \frac{R_L}{R_L^2 + (2n+1)^2 Z_{Lm(sin)}^2} \end{aligned} \tag{17}$$

By expanding the equation, we find that the power that can be obtained by the load under square wave excitation is:

$$\begin{aligned} P_{L(sq)} = \frac{8N^2K^2U_{in}^2}{\pi^2} \Bigg[&\frac{R_L}{R_L^2 + Z_{Lm(sin)}^2} + \frac{1}{9}\frac{R_L}{R_L^2 + 9Z_{Lm(sin)}^2} \\ &+ \frac{1}{25}\frac{R_L}{R_L^2 + 25Z_{Lm(sin)}^2} + \ldots \Bigg] \end{aligned} \tag{18}$$

For triangular waves, Eq. (7) can be expanded to give:

$$U(t) = \frac{8U_{in}}{\pi^2} \left(\sin\omega t + \frac{1}{9}\sin 3\omega t + \frac{1}{25}\sin 5\omega t + \ldots\right) \tag{19}$$

Eq. (11) can then be rewritten to give:

$$\begin{aligned} P_{L(tr)} &= \sum_{n=0}^{\infty} \left[\frac{8U_{in}}{(2n+1)^2\pi^2}\right]^2 \\ &\quad \times \frac{N^2 K^2 R_L}{2\left[R_L^2 + (2n+1)^4\omega^2 N^4 (1-K^2)^2 L_1^2\right]} \\ &= \frac{32N^2K^2U_{in}^2}{\pi^4} \sum_{n=0}^{\infty} \frac{1}{(2n+1)^4} \frac{R_L}{R_L^2 + (2n+1)^4 Z_{Lm(sin)}^2} \end{aligned} \tag{20}$$

By expanding this equation, we find that the power that can be obtained by the load under triangular wave excitation is:

$$P_{\mathrm{L(tr)}} = \frac{32N^2K^2U_{\mathrm{in}}^2}{\pi^4}\left[\frac{R_{\mathrm{L}}}{R_{\mathrm{L}}^2 + Z_{\mathrm{Lm(sin)}}^2} + \frac{1}{81}\frac{R_{\mathrm{L}}}{R_{\mathrm{L}}^2 + 81Z_{\mathrm{Lm(sin)}}^2} + \ldots\right] \tag{21}$$

According to Eq. (13), when the amplitudes of the higher-order harmonic components are large, there will be greater deviations in the MPTP calculated using the sinusoidal method. Additionally, a larger coupling coefficient K and a smaller primary inductance L_1 will result in a higher achievable maximum power. However, excessively small values of L_1 can increase the no-load current in the primary circuit, posing challenges in the primary circuit design. For the same load, a higher coupling coefficient in the loosely coupled transformer produces a higher maximum achievable power.

Therefore, to enhance the system's transmission capabilities, it is desirable to maximize the coupling coefficient of the loosely coupled transformer. While maintaining a fixed turns ratio, it is advisable to select a smaller number of turns for the primary winding to increase the upper limit for the maximum transmission power. It is important to note that the specific effects may vary with parameter variations, and further experimentation and analysis may be required.

III. DEMONSTRATION

In this section, numerical examples are presented using square waves and triangular waves as excitation sources to demonstrate the effectiveness of the proposed maximum power calculation method. In this example, the coil impedance is ignored. The system parameters considered here are: U_{in} =28 V; L_1 =8 μH; and L_2 =800 μH.

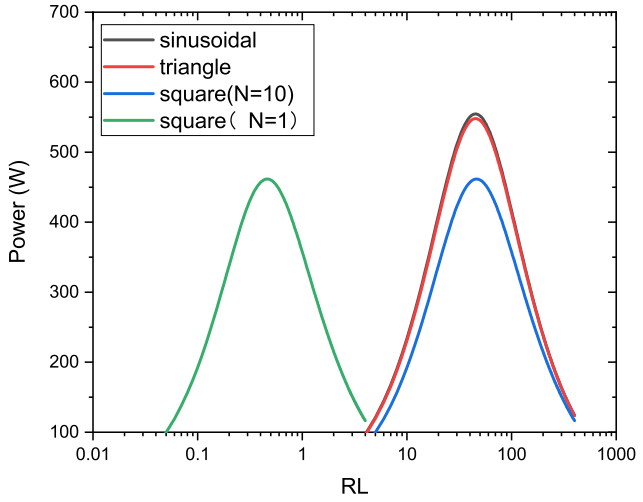

FIGURE 3. Load impedance and corresponding power.

Fig. 3 illustrates the variation of power with load impedance in the system when the coupling coefficient K is 0.8, and the frequency is 25 kHz. The simulation results are presented for square wave excitation with $N = 1$, where $L_1 = L_2$ =8 μH. It can be observed that the system exhibits a maximum power transfer point, and compared to sine and triangular wave excitations, the MPTP value is significantly smaller under square wave excitation. The choice of N does not impact the calculation results for the maximum power transfer, but it influences the corresponding impedance value at the maximum power point.

Following the outlined method above, a simple validation was conducted. According to Eq. (15), to control the error within 0.5%, at least 15 harmonics need to be considered. This ensures that the total signal power of the first 15 terms is greater than 99.5% of the total power. By performing a one-dimensional search on these curves, the MPTP and the corresponding load can be obtained. Comparisons between the proposed method, the sinusoidal assumption, and the simulation results are given in Tables 1-3.

TABLE 1. Comparison of MPTPs (K=0.8, square wave).

Frequency (kHz)	10	25	50	100
Simulated (w)	1325.0	529.99	265.05	132.62
Result of sinusoidal assumption (w)	1592.0	636.61	318.28	159.10
Proposed method (w)	1324.9	529.95	264.98	132.48
Error of traditional method (%)	20.151	20.117	20.083	19.967
Error of proposed method (%)	0.008	0.008	0.026	0.106

TABLE 2. Comparison of MPTPs (25 kHz, square wave).

K	0.6	0.7	0.8	0.9
Simulated (w)	167.69	286.43	529.99	1271.0
Result of sinusoidal assumption (w)	201.43	344.05	636.61	1527.0
Proposed method (w)	167.68	286.41	529.95	1270.8
Error of traditional method (%)	20.120	20.117	20.117	20.142
Error of proposed method (%)	0.006	0.007	0.008	0.016

Tables 1 and 2 show that when the excitation source is a square wave, the relative error decreases from 20% to within 0.2%. Table 3 shows that under triangular wave excitation, the error is also reduced from 1.2% to less than 0.1%. The above calculation results are within the expected range of accuracy.

TABLE 3. Comparison of MPTPs (25 kHz, triangular wave).

K	0.6	0.7	0.8	0.9
Simulated (w)	199.04	339.97	629.06	1509.0
Result of sinusoidal assumption (w)	201.13	344.05	636.61	1527.0
Proposed method (w)	199.03	339.97	629.05	1510.0
Error of traditional method (%)	1.050	1.200	1.199	1.193
Error of proposed method (%)	0.005	0.012	0.002	0.066

In conclusion, the proposed algorithm can be effectively utilized to calculate the maximum power transfer of coupled coils under non-sinusoidal excitation conditions with a notable improvement in the accuracy of the results, especially in cases characterized by large harmonic components in the input voltage.

IV. APPLICATION

In practical engineering applications, couplers exhibit inductance/capacitance resonance. This parasitic resonance, which cannot be accurately estimated in simulations, introduces richer harmonics and may result in the presence of distortion and overshoot waveforms. In this section, we present a real-world application case where an actual coupler is used to construct the experimental setup. In this experimental scenario, the calculation method proposed here is utilized to determine the system's MPTP and subsequently validate and compare the corrected results.

A. EXPERIMENTAL SETUP

The experimental setup for the testing system primarily comprises a 28 V power supply, a chopping wave drive circuit, a coupling structure, a rectification circuit, an oscilloscope, and an electronic load. The power supply provides electrical energy to the entire system. The constant current chopping wave drive circuit generates the excitation signal. The coupling structure is responsible for energy transfer. The rectification circuit then converts the received signal into a direct current power source. The oscilloscope facilitates current detection, while the electronic load operates in constant voltage mode to simulate a battery load. The schematic diagram of sampling points is illustrated in Fig. 4.

The experimental setup is depicted in Fig. 5. The power obtained by the load after transmission through the coupler is verified by measuring the voltage and current waveforms at the load end.

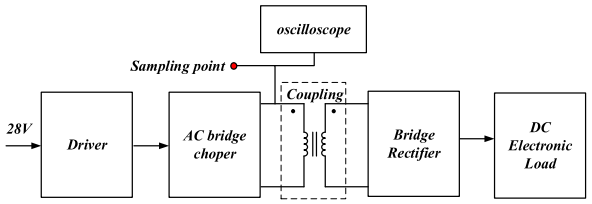

FIGURE 4. Schematic diagram of the sampling point.

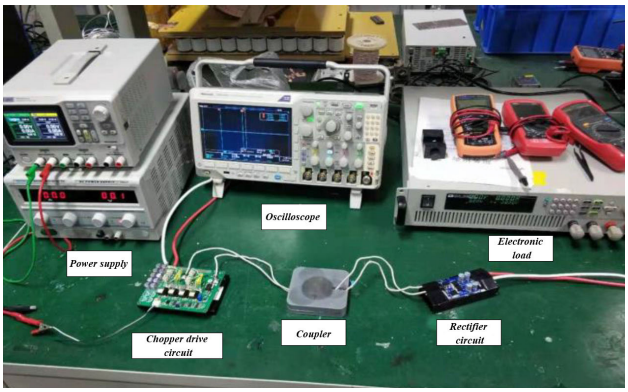

FIGURE 5. Experimental situation.

B. COUPLER PARAMETERS

This section describes the practical coupler, and the coupling coefficient and inductance parameters are determined for various coupler distances. An experimental setup is constructed using a magnetic induction coupler composed of ferrite and copper coils, as illustrated in Fig. 6.

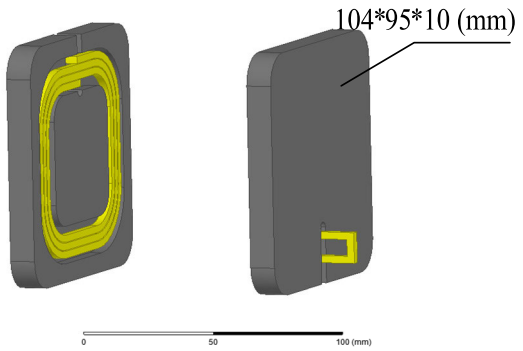

FIGURE 6. Coupler structure diagram.

A vector diagram of the magnetic induction intensity profile of the coupler obtained through simulations using Maxwell is shown in Fig. 7.

Fig. 7 illustrates the effective coupling region A and the leakage inductance region B in the coupler. The coupling coefficient, the self-inductance coefficient, and the leakage inductance parameters for the different coupler distances are obtained. In addition, due to changes in the coupling area, the coupling coefficient gradually decreases. An LCR meter was

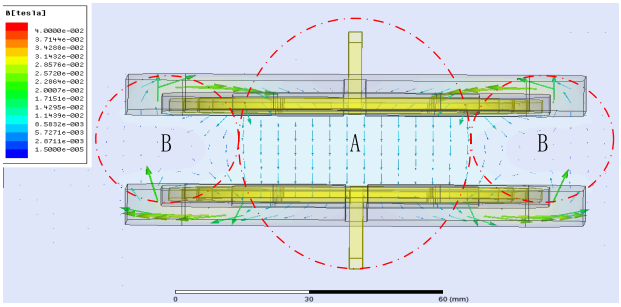

FIGURE 7. Magnetic field intensity distribution.

TABLE 4. Key coupler parameters.

Distance (mm)	1	2	3	4	5	6
K	0.98	0.95	0.92	0.89	0.86	0.82
L_{ET} (uH)	21.01	11.73	8.51	6.83	5.81	5.13
L_{Sim} (uH)	20.30	11.15	8.12	6.50	5.52	4.91
Distance (mm)	7	8	9	10	11	21
K	0.79	0.756	0.72	0.69	0.66	0.40
L_{ET} (uH)	4.64	4.27	3.99	3.77	3.59	2.8
L_{Sim} (uH)	4.47	4.09	3.82	3.61	3.43	2.76

utilized to measure the primary (secondary) self-inductance and coupling coefficient of the coupler at different distances. The simulation and measurement results are presented in Table 4. The simulated values and measured values of K are very close after rounding to two decimal places, and only the measured values are provided here. L_{Sim} denotes simulated values, while L_{ET} represents measured values.

C. MPTP IN ACTUAL ICPT SYSTEM

In this section, the system's maximum power is analyzed using a typical sampled waveform. In the experiment, the non-sinusoidal magnetic field excitation signal at point A in Fig. 4 is captured, and its frequency-domain characteristics are then analyzed using a fast Fourier transform (FFT).

Fig. 8 shows that there are differences between an ideal square wave and the sampled square wave obtained in practical applications. The actual waveform shows ringing with higher harmonic components.

Due to parasitic resonance, certain sub-harmonics experience increased amplitudes, while others are suppressed. As a result, the observed maximum power deviates from the ideal case. Subsequently, the constant current chopping circuit and the coupler were physically constructed, and real-time monitoring was performed using an oscilloscope and a current meter to ensure the experiment's reliability. The rectification circuit was then added to the experimental system, and the electronic load impedance was adjusted to simulate the load conditions during practical applications. Finally, the output voltage and current of the system were measured for various impedances, and the MPTP was calculated.

For experimentally sampled waveforms without specific analytical expressions, they can be imported into MATLAB

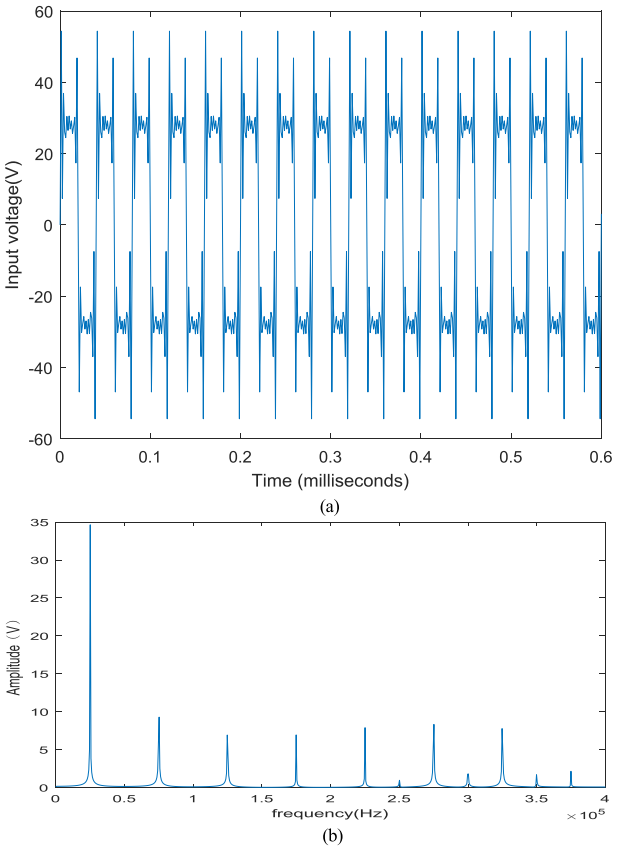

FIGURE 8. (a) Sampled waveform and (b) spectrogram.

for Fourier transformation. Subsequently, Eq. (12) proposed in this paper is employed for calculation. The maximum power is computed by truncating the waveform at the first 10, 15, 20, and 40 harmonics, and the percentage of total power is calculated as shown in Table 5.

TABLE 5. Harmonics and the percentage of total power.

Harmonics	10	15	20	40
Proportion (%)	96.78	99.40	99.59	99.95

The retained number of harmonics is determined based on the required accuracy. In the case of Fig. 8(a), where numerous harmonic components are present, the choice is made to retain the first 20 harmonic components. As the total power of the first 20 harmonics is already greater than 99.5%, it ensures that the computation guarantees an error within 0.5%.

Conduct a precise one-dimensional search on the truncated calculation results to determine the maximum power value and its corresponding impedance. Figs. 9 and 10 compare the maximum power and its corresponding matching impedance,

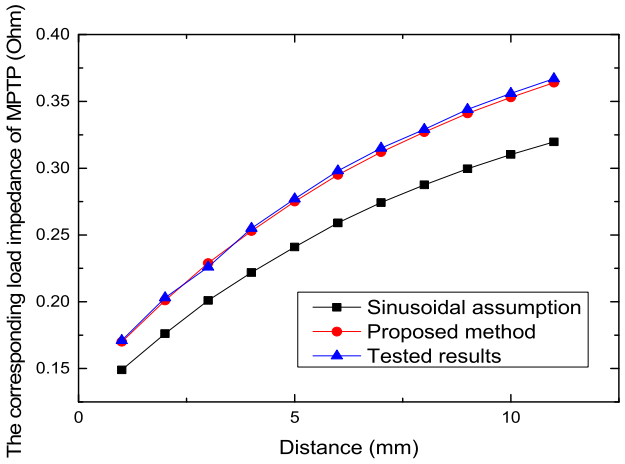

FIGURE 9. Impedance versus distance.

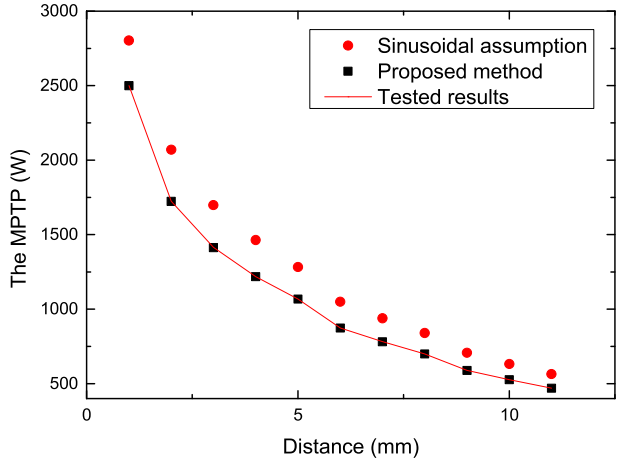

FIGURE 10. MPTP versus distance.

as calculated using the sinusoidal calculation method and the method proposed in this paper.

The experimental results indicate that an error occurs between the sinusoidal method and the experimental results, while the results from the calculation method proposed here are closer to the experimental results. Therefore, the method proposed in this paper should be used in practical applications.

V. CONCLUSION

This study presents a method for calculating the maximum power of ICPT systems under non-sinusoidal excitation. The main advantage of this method is its suitability for arbitrary excitation waveforms. Moreover, the superiority of this method becomes more pronounced as the excitation voltage deviates further from a sinusoidal waveform, i.e., when there is a larger harmonic component in the input voltage.

However, it is essential to acknowledge that this study has some limitations. Firstly, the proposed method is only applicable to scenarios without resonance compensation. Secondly, the method proposed in the paper may need to consider the introduction of time-frequency analysis when dealing with variable-frequency signals. Then, for non-resistive or nonlinear load scenarios, the current method may require further incorporation of equivalent impedance techniques to more accurately simulate the response of the system. Additionally, the modeling of transformers only considers the case of unsaturated magnetic cores.

It is important to note that some of the experimental results in this study are solely used for theoretical validation. In practical applications, factors such as steady-state operation, heat dissipation, and safety should be considered to determine the maximum transmission power of the system.

In terms of applications, this method provides valuable insights into the design and optimization of ICPT systems under non-sinusoidal excitation, especially in real-world scenarios where maximum power transfer is crucial. Future work should consider incorporating time-frequency analysis into variable-frequency signals and employing equivalent impedance techniques to deal with non-resistive or nonlinear loads.

Overall, despite some limitations, future research efforts aimed at improvement and expansion can enhance its applicability and provide comprehensive support for the design and optimization of wireless power transfer systems.

REFERENCES

[1] Q. Yang, H. Chen, G. Xu, M. Sun, and W. Fu, "Research progress in contactless power transmission technology," *Trans. China Electrotech. Soc.*, vol. 25, no. 7, pp. 6–13, Jul. 2010.

[2] Z. Yan, Y. Zhang, T. Kan, F. Lu, K. Zhang, B. Song, and C. C. Mi, "Frequency optimization of a loosely coupled underwater wireless power transfer system considering eddy current loss," *IEEE Trans. Ind. Electron.*, vol. 66, no. 5, pp. 3468–3476, May 2019.

[3] K. Qiao, P. Sun, E. Rong, J. Sun, H. Zhou, and X. Wu, "Anti-misalignment and lightweight magnetic coupler with H-shaped receiver structure for AUV wireless power transfer," *IET Power Electron.*, vol. 15, no. 16, pp. 1843–1857, Jul. 2022.

[4] Y. Jang and M. M. Jovanovic, "A contactless electrical energy transmission system for portable-telephone battery chargers," *IEEE Trans. Ind. Electron.*, vol. 50, no. 3, pp. 520–527, Jun. 2003.

[5] Q. Chen, S. C. Wong, C. K. Tse, and X. Ruan, "Analysis, design, and control of a transcutaneous power regulator for artificial hearts," *IEEE Trans. Biomed. Circuits Syst.*, vol. 3, no. 1, pp. 23–31, Feb. 2009.

[6] H.-D. Lang and C. D. Sarris, "Optimal design of implants for magnetically mediated hyperthermia: A wireless power transfer approach," *J. Appl. Phys.*, vol. 122, no. 12, Sep. 2017, Art. no. 124701.

[7] J.-Y. Lee and B.-M. Han, "A bidirectional wireless power transfer EV charger using self-resonant PWM," *IEEE Trans. Power Electron.*, vol. 30, no. 4, pp. 1784–1787, Apr. 2015.

[8] C. Hu, Y. Sun, Z. Wang, C. Tang, and Q. Xiong, "Design of magnetic coupler for EVs' wireless charging," *Int. J. Appl. Electromagn. Mech.*, vol. 43, no. 3, pp. 195–205, Aug. 2013.

[9] F. Yang, J. Jiang, C. Sun, A. He, W. Chen, Y. Lan, and K. Song, "Efficiency improvement of magnetic coupler with nanocrystalline alloy film for UAV wireless charging system with a carbon fiber fuselage," *Energies*, vol. 15, no. 22, p. 8363, Nov. 2022.

[10] A. F. A. Aziz, M. F. Romlie, and Z. Baharudin, "Review of inductively coupled power transfer for electric vehicle charging," *IET Power Electron.*, vol. 12, no. 14, pp. 3611–3623, Oct. 2019.

[11] C.-Y. Xia, N. Jia, and Y.-H. Zhuang, "Research on power transmission capacity of U-magnetic core structure ICPT system," *J. Electr. Eng. Technol.*, vol. 33, no. 8, pp. 7–10, Aug. 2014.

[12] X. Liu, Y. Xu, B. Peng, T. Sun, and M. Jia, "Study on magnetically-coupled bi-module wireless power transfer," *Trans. China Electrotech. Soc.*, vol. 30, no. 11, pp. 53–59, Jun. 2015.

[13] M. Xue, Q.-X. Yang, Y. Li, X. Zhang, and W. Liu, "The study of load characteristic in wireless energy transfer system based on EM coupling resonance," *Trans. China Electrotech. Soc.*, vol. 28, no. 2, pp. 28–34, Jan. 2013.
[14] A. Kurs, A. Karalis, R. Moffatt, J. D. Joannopoulos, and P. Fisher, "Wireless power transfer via strongly coupled magnetic resonances," *Science*, vol. 317, no. 5834, pp. 83–86, Jul. 2007.
[15] F. Huo, Y. Li, J. Wan, M. Wang, and J. Liu, "Optimal working state tracking method and experiments on inductive contactless power transmission system," *IET Power Electron.*, vol. 13, no. 12, pp. 2562–2568, Jul. 2020.
[16] Z. Zhang, K. T. Chau, C. Liu, C. Qiu, and F. Lin, "An efficient wireless power transfer system with security considerations for electric vehicle applications," *J. Appl. Phys.*, vol. 115, no. 17, p. 17, May 2014.
[17] D. Huang, Y. Urzhumov, D. R. Smith, K. Hoo Teo, and J. Zhang, "Magnetic superlens-enhanced inductive coupling for wireless power transfer," *J. Appl. Phys.*, vol. 111, no. 6, Mar. 2012, Art. no. 064902.
[18] S. D. Huang, Z. Q. Li, and Y. Li, "Transfer efficiency analysis of magnetic resonance wireless power transfer with intermediate resonant coil," *J. Appl. Phys.*, vol. 115, no. 17, p. 17, May 2014.
[19] A. I. Mahmood, S. K. Gharghan, M. A. Eldosoky, and A. M. Soliman, "Near-field wireless power transfer used in biomedical implants: A comprehensive review," *IET Power Electron.*, vol. 15, no. 16, pp. 1936–1955, Jul. 2022.
[20] S. Roy, A. N. M. W. Azad, S. Baidya, M. K. Alam, and F. Khan, "Powering solutions for biomedical sensors and implants inside the human body: A comprehensive review on energy harvesting units, energy storage, and wireless power transfer techniques," *IEEE Trans. Power Electron.*, vol. 37, no. 10, pp. 12237–12263, Oct. 2022.
[21] H. H. Wu, A. Gilchrist, K. D. Sealy, and D. Bronson, "A high efficiency 5 kW inductive charger for EVs using dual side control," *IEEE Trans. Ind. Informat.*, vol. 8, no. 3, pp. 585–595, Aug. 2012.
[22] N. Davister, F. Henrotte, F. Frebel, and C. Geuzaine, "Multiple resonance prediction through lumped-parameter modeling of transformers in high frequency applications," *IEEE Trans. Magn.*, vol. 59, no. 6, pp. 1–4, Jun. 2022.
[23] X. Mou, D. T. Gladwin, R. Zhao, and H. Sun, "Survey on magnetic resonant coupling wireless power transfer technology for electric vehicle charging," *IET Power Electron.*, vol. 12, no. 12, pp. 3005–3020, Sep. 2019.
[24] K. Fotopoulou and B. W. Flynn, "Wireless power transfer in loosely coupled links: Coil misalignment model," *IEEE Trans. Magn.*, vol. 47, no. 2, pp. 416–430, Feb. 2011.
[25] A. A. S. Mohamed, S. An, and O. Mohammed, "Coil design optimization of power pad in IPT system for electric vehicle applications," *IEEE Trans. Magn.*, vol. 54, no. 4, pp. 1–5, Apr. 2018.
[26] Q. Xu, Q. Hu, H. Wang, Z.-H. Mao, and M. Sun, "Optimal design of planar spiral coil for uniform magnetic field to wirelessly power position-free targets," *IEEE Trans. Magn.*, vol. 57, no. 2, pp. 1–9, Feb. 2021.
[27] Y. Yamamoto, I. Hodaka, K. Yamaguchi, and T. Hirata, "Using non-sinusoidal inputs for efficient wireless power transmission," in *Proc. Int. Conf. Circuits Syst. Signal Process. Commun. Comput.*, 2014, pp. 58–60.
[28] K. Yamaguchi and T. Hirata, "Efficient wireless power transfer-resonance does not imply high efficiency," Private Communication.
[29] Y.-J. Guo, L.-F. Wang, Q.-W. Zhu, C. Liao, and J. Li, "Power and efficiency characteristics of electric vehicle wireless charging system based on non-sinusoidal input," *Trans. China Electrotech. Soc.*, vol. 30, no. S1, pp. 204–208, Sep. 2015.
[30] Y. Sun, Z.-J. Liao, Z.-H. Ye, C.-S. Tang, and P.-Y. Wang, "Determining the maximum power transfer points for MC-WPT systems with arbitrary number of coils," *IEEE Trans. Power Electron.*, vol. 33, no. 11, pp. 9734–9743, Nov. 2018.
[31] C. Liu, K. T. Chau, Z. Zhang, C. Qiu, W. Li, and T. W. Ching, "Wireless power transfer and fault diagnosis of high-voltage power line via robotic bird," *J. Appl. Phys.*, vol. 117, no. 17, p. 17, Apr. 2015.
[32] O. H. Stielau and G. A. Covic, "Design of loosely coupled inductive power transfer systems," in *Proc. Int. Conf. Power Syst. Technol.*, Perth, WA, Australia, 2000, pp. 85–90, Paper 00EX409.
[33] C. Duan, C. Jiang, A. Taylor, and K. Bai, "Design of a zero-voltage-switching large-air-gap wireless charger with low electric stress for electric vehicles," *IET Power Electron.*, vol. 6, no. 9, pp. 1742–1750, Nov. 2013.
[34] V. Cirimele, F. Freschi, L. Giaccone, L. Pichon, and M. Repetto, "Human exposure assessment in dynamic inductive power transfer for automotive applications," *IEEE Trans. Magn.*, vol. 53, no. 6, pp. 1–4, Jun. 2017.
[35] J. Sallan, J. L. Villa, A. Llombart, and J. F. Sanz, "Optimal design of ICPT systems applied to electric vehicle battery charge," *IEEE Trans. Ind. Electron.*, vol. 56, no. 6, pp. 2140–2149, Jun. 2009.
[36] Y. Wu, Q. Chen, X. Ren, and Z. Zhang, "Efficiency optimization based parameter design method for the capacitive power transfer system," *IEEE Trans. Power Electron.*, vol. 36, no. 8, pp. 8774–8785, Aug. 2021.
[37] J. Qi, "Analysis, design, and optimisation of an LCC/S compensated WPT system featured with wide operation range," *IET Power Electron.*, vol. 13, no. 9, pp. 1819–1827, Jul. 2020.

YUE XU was born in Mohe, Heilongjiang, China, in February 1995. She received the B.E. degree from the School of Electronic Engineering, Heilongjiang University, Heilongjiang, in 2017. She is currently pursuing the Ph.D. degree with the School of Aerospace Science and Technology, Xidian University, Xi'an, China. Her current research interests include electromagnetic propagation and wireless power transfer.

KAI XIE was born in Jiangxi, China, in November 1983. He received the B.E., M.S., and Ph.D. degrees from Xidian University, Shaanxi, China, in 2003, 2006, and 2014, respectively. In 2006, he joined Xidian University and became a Full Professor, in 2016. His research interests include plasma physics, EM propagation, and aerospace TT&C and communications.

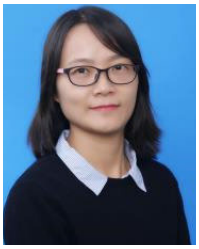

YAN LIU received the B.E. and M.S. degrees from Xidian University, Xi'an, China, in 2007 and 2009, respectively, and the Ph.D. degree in optics, photonics and image processing from École Centrale de Marseille, France, in 2014. Since 2014, she has been a Lecturer with the School of Aerospace Science and Technology, Xidian University. Her research interests include metamaterials, metasurfaces, EM propagation, and low frequency mechanical antennas.